Histological and histochemical characterization of the musk gland in forest musk deer (*Moschus berezovskii*): a preliminary study

Qianyi Wang,[1] Chunyu Han,[2] Dong Zhang,[3] Yuning Liu,[1] Yunyun Gao,[3] Haolin Zhang,[1] Defu Hu[3]

[1]Laboratory of Animal Physiology, College of Biological Sciences and Technology, Beijing Forestry University, Beijing
[2]Beijing Yanshe Biotechnology Development Company, Beijing
[3]School of Ecology and Nature Conservation, Beijing Forestry University, Beijing, China

ABSTRACT

Musk is a biologically valuable secretion from the musk gland of male musk deer, with significant economic and medicinal importance. Due to severe decline and depletion of wild musk deer population, captive breeding of musk deer has become the primary approach for sustainable musk production. So far, the histological structure and secretion mechanism of the musk gland remain incompletely understood. In this study, we employed histological and immunohistochemical (IHC) techniques, along with three-dimensional (3D) tissue reconstruction, to systematically analyze the cellular composition and secretory functions of the musk gland in forest musk deer (*Moschus berezovskii*). Our results revealed that the musk gland was primarily composed of acinar structures containing two distinct glandular cell (GC) types based on the histological observation. IHC results showed type I glandular cells (GCIs) predominantly expressed GALNT7 while type II glandular cells (GCIIs) mainly expressed BMP6. The 3D reconstruction demonstrated structural heterogeneity along the gland's longitudinal axis, with the proportion of the acinar area varying between 40% and 65%. This is the first time that a detailed 3D view of musk gland in forest musk deer has been shown, which provides essential histological insights into musk gland function in this species. These preliminary observations may provide useful groundwork for future investigations into the regulatory mechanisms of musk secretion.

Key words: forest musk deer; musk gland; immunohistochemistry; tissue structure; three-dimensional reconstruction.

Correspondence: Haolin Zhang, D.V.M., Laboratory of Animal Physiology, College of Biological Science and Technology, Beijing Forestry University, Beijing 100083, China. E-mail: haolinzhang@bjfu.edu.cn

Contributions: QW, data collection and analysis, manuscript original drafting; CH, sample collection; DZ, resources, project administration, methodology; YL, visualization, resources, investigation; YG, sample collection, resources, manuscript reviewing; DH, resources, project administration; HZ, supervision, manuscript reviewing and editing. All authors read and approved the final version of the manuscript and agreed to be accountable for all aspects of the work.

Conflict of interest: all authors declare no conflict of interest, and all authors confirm accuracy.

Ethical approval: this study design and animal experiments were conducted following the guidelines of the Animal Care and regulations of Beijing Forestry University, China (No. EAWC_BJFU_2025001).

Funding: this work was supported by 5·5 Engineering Research & Innovation Team Project of Beijing Forestry University (BLRC 2023C02) and Beijing Natural Science Foundation (6222042) and the National Natural Science Foundation of China (32270519).

Introduction

Musk, a secretion from musk gland of the male deer species within the family Moschidae,[1,2] is a valuable biological resource with applications in traditional Chinese medicine and perfumery.[3-5] Due to overexploitation and habitat loss, wild musk deer populations have experienced a significant decline,[6] leading to a reliance on captive breeding for sustainable musk production.[7] Currently, the primary species being farmed is the forest musk deer (*Moschus berezovskii*), which is also the main source of musk. Although both wild and farmed populations of forest musk deer have seen a relative increase, the musk production from farmed deer still fails to meet the market demand. Therefore, investigating the structure of the musk gland in forest musk deer and elucidating the mechanisms of musk secretion are of significant importance for both the conservation and sustainable utilization of musk deer resources.

The musk gland, located in the abdominal region of male musk deer, contains specialized glandular cells responsible for musk synthesis. Previous studies have described its general histological structure, identifying acinar cells within the glandular epithelium, which is surrounded by smooth muscle cells and interstitial cells.[8-10] Moreover, single-nucleus sequencing has revealed two distinct types of glandular cells in the musk gland, characterized by the gene markers *Galnt7* and *Bmp6*, respectively.[11] However, the detailed cytoarchitecture and specific roles of different glandular cell types remain incompletely understood.

Three-dimensional tissue reconstruction technology provides a feasible approach for visualizing the spatial structure of the musk gland. By performing z-stacking of serial histological sections, we successfully generated a three-dimensional reconstruction. This optical sectioning technique effectively overcomes the limitations of conventional histochemical analysis by enabling improved visualization of deep tissue regions and mitigating technical challenges.[12-14] This study aims to systematically characterize the tissue structure and cellular composition of the musk gland in the forest musk deer. By combining hematoxylin-eosin (H&E) staining, immunohistochemistry (IHC), and three-dimensional (3D) reconstruction, we seek to elucidate the spatial distribution of glandular cells in the musk gland. These findings will provide a structural basis for further molecular investigations and potential biotechnological applications in musk production.

Materials and Methods

Sample collection

The musk gland tissue was collected from a captive adult male forest musk deer in October, which is provided by the breeding farm of Yanshe Biotechnology Development Company, Beijing, China. The animal was housed in an outdoor environment, with 1-2 individuals per enclosure. All experimental procedures were approved by the Animal Ethic Committee at Experimental Center of Beijing Forestry University (approval No. EAWC_BJFU_2025001), in accordance with the guidelines. The musk gland tissue was fixed overnight at room temperature with 4% paraformaldehyde fix solution for histological and immunohistochemical observations.

Histology

The fixed musk gland sample was dehydrated through a graded ethanol series, cleared with xylene, and embedded in paraffin wax.[15] Serial sections (5 µm thickness) were obtained using a rotary microtome, mounted on glass slides, and dried at 37°C for overnight. H&E staining was performed to assess the general tissue architecture, following standard protocols. Stained sections were visualized using an Olympus BX53 photomicroscope (Olympus, Tokyo, Japan) equipped with PlanN (4-20×) or UPlanFLN (40×) objectives.

Immunohistochemistry

The immunohistochemical protocol was described in a previous study.[16] Briefly, paraffin-embedded sections were deparaffinized and rehydrated through a descending ethanol gradient. Antigen retrieval was performed using citric acid buffer (pH 6.0), heated at 100°C for 5 min, 80°C for 5 min and 40°C for 5 min., then followed by blocking with 3% hydrogen peroxide for 30 min after cooling. The sections were incubated overnight at 4°C with primary antibodies: rabbit polyclonal anti-GALNT7 (13962-1-AP, Proteintech Group, Inc., Rosemont, IL, USA) and anti-BMP6 (55421-1-AP, Proteintech Group). Goat anti-rabbit IgG/HRP secondary antibody (bs-0295G-HRP, Bioss Biotechnology, Beijing, China) was applied at 37°C for 40 min. The primary antibodies were diluted at a concentration of 1:200 and the secondary antibody was diluted at a concentration of 1:1000. The slide rinsing between steps was performed with phosphate buffered saline (PBS) at a concentration of 10 mM. Immunoreactivity was visualized using 3,3'-diaminobenzidine (DAB) chromogen solution (0.02% w/v DAB in Tris-HCl buffer pH7.6 plus 17 µL 30% H_2O_2) for 1 min, followed by hematoxylin counterstaining. Stained sections were also visualized using an Olympus BX53 photomicroscope (Olympus, Tokyo, Japan) equipped with PlanN (4-20×) or UPlanFLN (40×) objectives. Six fields (with certain intervals) were randomly sampled from each tissue to analyze the proportion of positive regions. At the same time, each entire sheet was scanned and analyzed. The maximum error of the obtained results was discarded and the average value was calculated, and the quantification of staining intensity was automatically measured with the plugin of IHC profiler in Fiji software.[17,18]

Three-dimensional reconstruction and result analysis

Consecutive sections were grouped at 30 µm intervals, with corresponding sections selected from each group for whole-slide scanning using ImageView (Suzhou Jingtong Instrument Co., Ltd., Suzhou, China). A section sequence was generated using the 3DHISTECH's Slide Converter (3D HISTECH Ltd., Budapest, Hungary) and CaseViewer (3D HISTECH Ltd., Budapest, Hungary), The pictures are arranged in sequence in CaseViewer format and can be calibrated automatically. Tissue images were aligned, processed, and stacked along the z-axis in the brightfield mode, with a thickness setting of 6 µm. The 3D reconstruction results were visualized using Voloom v3.0.0.0 (microDimensions, Munich, Germany). Statistical analysis and chart generation were performed with GraphPad Prism 10 (GraphPad Software Inc, CA, USA).

Results

Histological analysis

The tissue specimen obtained from the forest musk deer's gland measured approximately 4 × 3 cm in cross-sectional dimensions. Histological preparation yielded consecutive transverse sections encompassing a total tissue depth of 670 µm (Figure 1a). The structure of the musk gland was broadly divided into three parts: the acinar region, the ductal region, and the interstitial region

(Figure 1 b,f). The acinar region was predominantly characterized by acinar structures, which constituted the principal cellular organization within the musk gland (Figure 1 c,e). The diameter of individual acini ranged from about 60 to 180 µm (measured along the long axis for irregularly shaped structures). Moreover, the distribution of acini in the outer glandular regions, located near the glandular periphery, was denser than that in the inner glandular regions. A layer of myoepithelial cells with elongated nuclei and a flattened morphology encircles each acinus, marking the boundary between the acinar and stromal regions (Figure 1 c,e).

Based on cell nuclei location and cell morphology, glandular cells in the musk gland of forest musk deer were categorized into two types: type I glandular cells (GCIs) and type II glandular cells (GCIIs). GCIs were the predominant epithelial cells in the glandular epithelium, characterized by irregular columnar contours and relatively small oval nuclei. In contrast, GCIIs were scattered within the glandular epithelium, exhibiting round or ovoid shapes with larger nuclear and cytoplasmic volumes (Figure 1 c,e).

The inter-acinar spaces containing stromal components formed the interstitial region, which was composed of various types of interstitial cells (Figure 1 c,e). The ductal region primarily consisted of secretory ducts, lined by a single layer of ductal epithelial cells surrounding the lumen (Figure 1 d,f). The ductal system was concentrated in the central tissue region, facilitating the transport of secretory products (Figure 1f).

Immunohistochemical analysis

As the marker of acinar cells, the immunostaining of GALNT7 and BMP6 was examined in the musk gland (Figures 2 and 3). The positive staining of GALNT7 and BMP6 was mainly observed in the glandular cells (Figure 2a and Figure 3a). At the overall level, glandular cells located in the outer layer regions of musk gland exhibited generally stronger immunoreactivity than those located in the inner layer regions (Figure 2 b,c and Figure 3 b,c). In the glandular cells of the inner layer region, GCIs exhibited relatively strong GALNT7 immunoreactivity, whereas GCIIs showed weaker GALNT7 staining (Figure 2d). In contrast, GCIs displayed relatively weak BMP6 immunoreactivity, while GCIIs demonstrated stronger BMP6 staining (Figure 3d). In addition, no positive staining for GALNT7 or BMP6 was observed in the ductal epithelial cells, interstitial cells, or myoepithelial cells (Figure 2 b-d and Figure 3 b-d; Table 1). The IHC results for GALNT7 or BMP6 were also quantified with ImageJ, as shown in Figure 2e and Figure 3e. The quantitative analysis of IHC staining for GALNT7 revealed that 4% of the cells exhibited high positivity, while 12.83% and 29.66% showed positive and low positive staining, respectively (Figure 2e). Additionally, 53.51% of the cells were negative for GALNT7 expression (Figure 2e). Similarly, the quantitative analysis of BMP6 immunohistochemical staining showed that 2.45% of the cells exhibited high positivity, while 14.96% and 38.13% displayed positive and low positive staining, respectively (Figure 3e). Moreover, 44.46% of the cells were negative for BMP6 expression (Figure 3e).

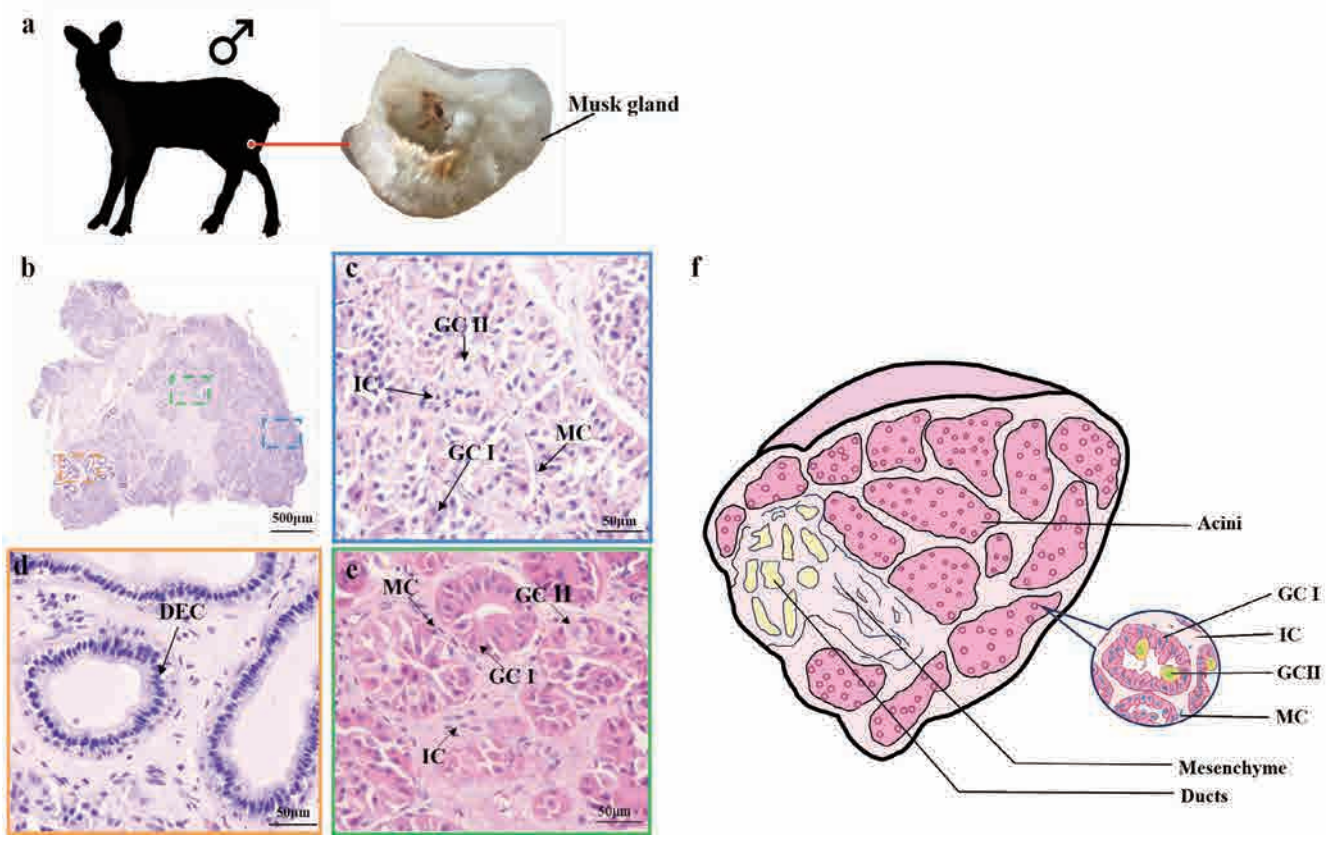

Figure 1. Histological analysis of the musk gland in forest musk deer. **a**) The musk gland tissue originated from the male forest musk deer (M. berezovskii). **b**) Overview of the histological structure of the musk gland. **c**) Magnified view of acinar regions near the periphery of the musk gland tissue. **d**) Magnified view of the ductal area within the musk gland tissue. **e**) Magnified view of acinar regions in the central part of the musk gland tissue. **f)** Schematic diagram of the musk gland based on histological observations. GC, glandular cells; GCI, type I glandular cells; GCII, type II glandular cells; IC, interstitial cells; MC, myoepithelial cells; DEC, ductal epithelial cells.

Three-dimensional reconstruction

3D histological reconstruction was performed using serial section alignment and volumetric modeling. This approach provided a detailed three-dimensional architectural representation of the musk gland (Figure 4). The histomorphometric analysis of musk gland cross-sections revealed structural heterogeneity along the longitudinal axis. Progressive spatial analysis demonstrated a gradual reduction and eventual disappearance of ductal areas, accompanied by a centripetal expansion of interstitial regions toward the tissue core (Figure 4c). The proportion of the acinar area varied between 40% and 65% within the musk gland (Figure 4d). 3D model and video can be found on online *via* the links https://doi.org/10.6084/m9.figshare.28620986.v1 (mdv.), https://doi.org/10.6084/m9.figshare.28620995.v1 (mdv.), https://doi.org/10.6084/m9.figshare.28623104.v1 (videos).

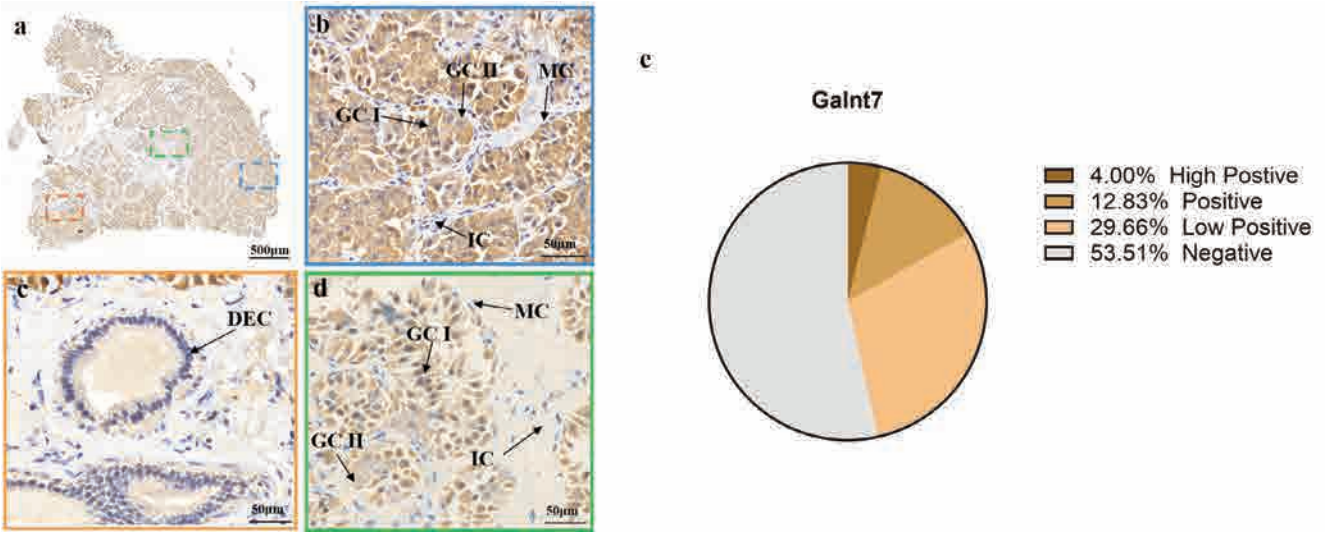

Figure 2. Immunohistochemical results of GALNT7 within the musk gland. **a**) Overview of immunohistochemical staining of GALNT7 in the musk gland. **b**) Immunostaining of GALNT7 in the acinar regions near the periphery of the musk gland tissue. **c**) Immunostaining of GALNT7 in the ductal area within the musk gland tissue. **d**) Immunostaining of GALNT7 in the acinar regions in the central part of the musk gland tissue. (**e**) Evaluation of GALNT7 immunostaining in the musk gland tissue. GC, glandular cells; GCI, type I glandular cells; GCII, type II glandular cells; IC, interstitial cells; MC, myoepithelial cells; DEC, ductal epithelial cells.

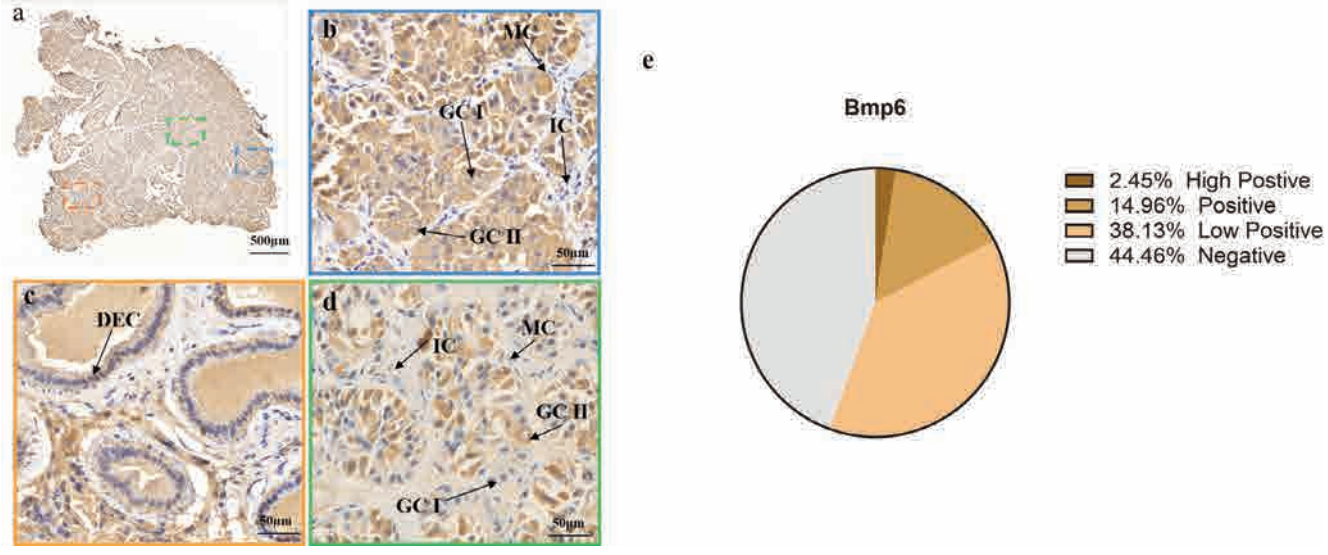

Figure 3. Immunohistochemical results of BMP6 within the musk gland. **a**) Overview of immunohistochemical staining of BMP6 in the musk gland. **b**) Immunostaining of BMP6 in the acinar regions near the periphery of the musk gland tissue. **c**) Immunostaining of BMP6 in the ductal area within the musk gland tissue. **d**) Immunostaining of BMP6 in the acinar regions in the central part of the musk gland tissue. **e**) Evaluation of BMP6 immunostaining in the musk gland tissue. GC, glandular cells; GC I, type I glandular cells; GC II, type II glandular cells; IC, interstitial cells; MC, myoepithelial cells; DEC, ductal epithelial cells.

Discussion

Investigating the structural organization of the musk gland is of paramount importance for elucidating the physiological mechanisms underlying musk secretion, which has significant implications for both biomedical research and wildlife conservation. In our study, histological staining revealed distinct zonal characteristics within the musk gland, with region-specific distributions of glandular cells in the acinar region, duct epithelial cells in the sectary duct region, and interstitial cells in the interstitial region. These findings are consistent with earlier observations reported by Chen *et al.*[19] and Yang *et al.*[20] Those results confirm the glandular cells, myoepithelial cells and interstitial cells presenting in the musk gland, which validated the reliability of our histological approach. Glandular cells are generally considered as the main cells responsible for the musk production in the musk gland of forest deer.[21-23] Single-nucleus RNA and ATAC sequencing of the musk gland identified 13 distinct cell types, including two glandular cell populations characterized by the expression of the genetic markers GALNT7 and BMP6.[11] In our current study, we also found two types of glandular cells presenting in the musk gland based on the cell morphology. Moreover, the immunoactivity of GALNT7 was mainly presented in the GCIs and the positive staining of BMP6 was mainly observed in the GCIIs, especially in the inner zone of glandular epithelium. Those data enhance the link between the cellular gene expression and cell localization in the musk gland. Furthermore, the immunoreactive density of GALNT7 or BMP6 varied from inner to outer glandular epithelium, indicating the protein expression differences among those cells. Together, these results suggest the potential spatial heterogeneity among different types of glandular cells. Future studies employing spatial transcriptomics and other advanced techniques are needed to further investigate the classification and distribution of acinar cells within the scent gland.

The current study is the first to apply three-dimensional histological reconstruction to delineate the detailed spatial architecture of the musk gland. Our analysis revealed significant structural heterogeneity along the gland's longitudinal axis. Notably, the progressive loss of ductal regions, combined with the centripetal expansion of interstitial areas toward the core, suggests that dis-

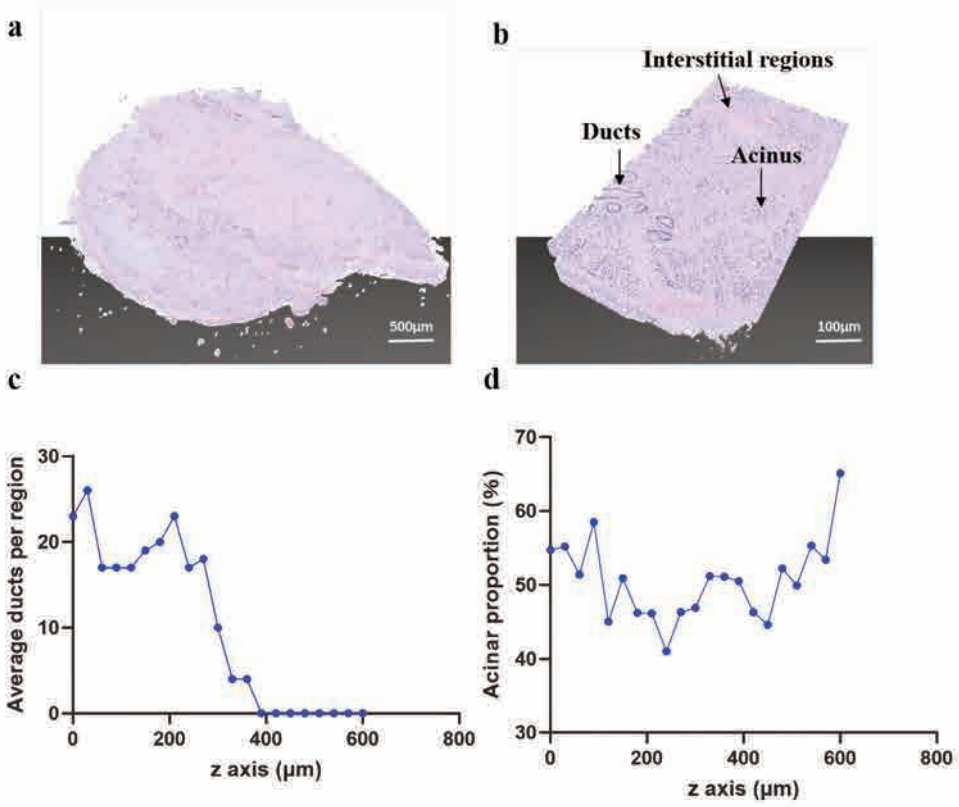

Figure 4. a,b). Different magnification of 3D reconstruction with musk gland sections based on the H&E staining. **c**) The average ducts per section along with the z axis in the 3D view of musk gland. **d**) The proportion of acinar area per section along with the z axis in the 3D view of musk gland.

Table 1. The protein expression in different type of cells in the musk gland of forest musk deer.

Markers	GCI	GCII	IC	MC
GALNT7	+ +	+	—	—
BMP6	+	+ +	—	—

GCI, type I glandular cells; GCI, type II glandular cells; IC, interstitial cells; MC, myoepithelial cells; +, positive staining; ++, strong positive staining; -, negative staining.

tinct zones within the gland may have unique functional roles. Moreover, the observed variation in acinar area (from 40% to 65%) implies that the secretory capacity differ across regions. These findings are consistent with previous studies on exocrine glands tissues, which have demonstrated that spatial heterogeneity plays a critical role in functional specialization. For example, research on salivary and lacrimal has shown that variations in acinar and ductal composition can be closely correlated with differences in secretory output and cellular metabolism.[24-26] In addition, comparative transcriptomic analyses between the musk gland and sebaceous gland have confirmed similarities with other exocrine tissues, further supporting the notion that spatial organization is integral to glandular function.[27,28] Like the physiological structure patterns of other exocrine glands, the musk gland also has a branched structure which transports secreta produced in the acini through a tree-like network of ducts,[29-32] while the acini composed of differentiated epithelial cells that are able to differentiate to form functional units.[33,34]

Beyond the forest musk deer (*M. berezovskii*), chemosignal production *via* specialized scent glands is a convergent evolutionary trait observed in phylogenetically diverse taxa facing similar ecological pressures, such as territory marking, sexual attraction, or predator deterrence. The present detailed histological characterization of the forest musk deer musk gland enables meaningful cross-species comparisons. Although differing in anatomical location and developmental origin, the musk-secreting structures of the Chinese forest musk deer (current study), the muskrat (*Ondatra zibethicus*), and the masked palm civet (*Paguma larvata*) share core functional adaptations.[35-37] The musk glands of these three musk-secreting animals have the hypertrophied glandular acini, which could be optimized for high-volume secretion storage. The glandular cells in the musk glands of these musk-secreting animals are the main cells synthesizing the complex lipid and protein compounds, which may function as pheromones to mediate chemical communication. In addition to these similarities, notable differences in the histological structure also exist. For example, In the forest musk deer, glandular epithelial cells exhibit a highly organized, ring-like arrangement around a lumen, secreting liquid-phase musk precursors into musk gland sacs. Critically, within the musk gland sacs, microbial communities facilitate a secondary fermentation process, transforming the liquid secretion into the mature, solidified musk product.[38,39] Conversely, in *O. zibethicus*, the glandular cells do not form a well-defined, patent lumen:[35,36] secretions are directly released into the branching ductal networks where they remain in a liquid state until being discharged externally.[35,36]

Given the status of the forest musk deer as a Class I nationally protected animal in China, obtaining biological samples presents substantial legal and ethical challenges, restricting both sample size and population representation. This constraint inherently limits the generalizability of our findings, as potential variations across individuals, seasonal fluctuations, and population-level diversity remain unexplored. Despite these limitations, this meticulously collected sample represents a rare and scientifically valuable resource. Our study provides the 3D structure and detailed morphological and histochemical characterization of the musk gland in the forest musk deer. This preliminary investigation establishes an essential morphological foundation and would support the biochemical, molecular and multi-omics investigation for the future study.

Collectively, our study not only contributes new histological data of the musk gland but also advances our understanding by introducing a novel 3D perspective. These observations may provide useful groundwork for future investigations into the regulatory mechanisms governing musk secretion.

Acknowledgments

Thanks to the farmers in Yanshe Biotechnology Development Company, who helped to collect the musk gland tissues.

References

1. Fan MY, Zhang MS, Shi MH, Zhang TX, Qi L, Yu J, et al. Sex hormones play roles in determining musk composition during the early stages of musk secretion by musk deer (Moschus berezovskii). Endocr J 2018;65:1111-20.
2. Yoshikawa K, Deguchi J, Hu JY, Lu HY, Matsunami H. An odorant receptor that senses four classes of musk compounds. Curr Biol 2022;32:5172-79.
3. Jie H, Feng XL, Zhao GJ, Zeng DJ, Zhang CL, Chen Q. Research progress on musk secretion mechanism of forest musk deer. Chin J Chin Mater Med 2014;39:4522-5.
4. Wang Y, Sun M, Chang F, Wang J, Wang Y, Tang J, et al. The essential differences in microbial and chemical components of musk of different qualities secreted by captive male forest musk deer (Moschus berezovskii). Microb Biotechnol 2022;15:1783-94.
5. Ding M, Fan JL, Huang DF, Jiang Y, Li MN, Zheng YQ, et al. From non-targeted to targeted GC-MS metabolomics strategy for identification of TCM preparations containing natural and artificial musk. Chin Med 2022;17:41.
6. Jiang F, Zhang JJ, Gao HM, Cai ZY, Zhou XW, Li S, Zhang TZ. Musk deer (Moschus spp.) face redistribution to higher elevations and latitudes under climate change in China. Sci Total Environ 2020;704:135335.
7. Fan ZX, Li WJ, Jin JZ, Cui K, Yan CC, Peng CJ, et al. The draft genome sequence of forest musk deer (Moschus berezovskii). Gigascience 2018;7:giy038.
8. Hong TT, Liu CM, Wang SH,' Dong XG, Ren ZJ. The Histostructures of musk gland at different ages and periods in forest musk deer. Chin J Zool 2023;58:742 -50.
9. Feng WH, You YX, Yong HY, Li GR, Gu QX. Histological observation of musk gland in forest musk deer. Chin J Zool 1981;1981:33-5.
10. Feng H, Feng TY, Mo YD, Sun SL, Wang L, Lu CB, et al. Integrated multi-omics analysis reveals insights into Chinese forest musk deer (Moschus berezovskii) genome evolution and musk synthesis. Front Cell Dev Biol 2023;11:1156138.
11. Liu CM, Hong TT, Yu L, Chen Y, Wang SH, Ren ZJ. Single-nucleus RNA and ATAC sequencing uncovers the molecular and cellular characteristics in the musk gland of Chinese forest musk deer (Moschus berezovskii). FASEB J 2023;37:e22742.
12. Haddad TS, Friedl P, Farahani N, Treanor D, Zlobec I, Nagtegaal I. Tutorial: methods for three-dimensional visualization of archival tissue material. Nat Protoc 2021;16:4945-62.
13. Liu HX, Zhu RY, Liu CY, Ma RF, Wang LL, Chen BB, et al. Evaluation of decalcification techniques for rat femurs using HE and immunohistochemical staining. Biomed Res Int 2017;2017:9050754.
14. Cardiff RD, Miller CH, Munn RJ. Manual hematoxylin and eosin staining of mouse tissue sections. Cold Spring Harb Protoc 2014;2014:655-8.
15. Zhang TX, Peng D, Qi L, Li WX, Fan MY, Shen JC, et al. Musk gland seasonal development and musk secretion are regulated by the testis in muskrat (Ondatra zibethicus). Biol Res 2017;50:10.
16. Guo SM, Yang WJ, Chen D, Ren BL, Guo L, Wang X, et al. The effects of low ambient temperature on steroidogenesis and

mitochondrial functions in the testes of wild ground squirrels (Spermophilus dauricus). Comp Biochem Physiol A Mol Integr Physiol 2024;290:111585.
17. Schindelin J, Arganda-Carreras I, Frise E, Kaynig V, Longair M, Pietzsch T, et al. Fiji: an open-source platform for biological-image analysis. Nat Methods 2012;9:676-82.
18. Varghese F, Bukhari AB, Malhotra R, De A. IHC Profiler: an open source plugin for the quantitative evaluation and automated scoring of immunohistochemistry images of human tissue samples. PLoS One 2014;9:e96801.
19. Chen M, Jie H, Xu ZX, Ma T, Lei MY, Zeng DJ, et al. Isolation, primary culture, and morphological characterization of gland epithelium from forest musk deer (Moschus berezovskii). In Vitro Cell Dev Biol Anim 2018;54:545-8.
20. Yang JM, Peng GF, Shu F, Dong DQ, Zheng XL, Zhu C, et al. Characteristics of steroidogenesis-related factors in the musk gland of Chinese forest musk deer (Moschus berezovskii). J Steroid Biochem Mol Biol 2021;212:105916.
21. Liu CM, Hong TT, Wang SH, Dong XG, Ren ZJ. Research progress on molecular mechanism of musk secretion in forest musk deer. Chin J Zool 2022;57:152-8.
22. Liu CM, Hong TT, Yu L, Chen Y, Dong XG, Ren ZJ. Single-nucleus multiomics unravels the genetic mechanisms underlying musk secretion in Chinese forest musk deer (Moschus berezovskii). Int J Biol Macromol 2024;279:135050.
23. Wang T, Yang MS, Shi X, Tian SL, Li Y, Xie WQ, et al. Multiomics analysis provides insights into musk secretion in muskrat and musk deer. Gigascience 2025;14:giaf006.
24. Rocha EM, Alves M, Rios JD, Dartt DA. The aging lacrimal gland: changes in structure and function. Ocul Surf 2008;6:162-74.
25. Bannier-Hélaouët M, Post Y, Korving J, Trani Bustos M, Gehart H, Begthel H, et al. Exploring the human lacrimal gland using organoids and single-cell sequencing. Cell Stem Cell 2021;28:1221-32.
26. Chibly AM, Aure MH, Patel VN, Hoffman MP. Salivary gland function, development, and regeneration. Physiol Rev 2022;102:1495-552.
27. Li L, Cao HR, Yang JM, Jin TQ, Ma YX, Wang Y, et al. Genetic and histological relationship between pheromone-secreting tissues of the musk gland and skin of juvenile Chinese forest musk deer (Moschus berezovskii Flerov, 1929). J Zhejiang Univ Sci B 2023;24:807-22.
28. Liu CM, Hong TT, Zhao CC, Xue T, Wang SH, Ren ZJ. Single-nucleus transcriptomics and chromatin accessibility analysis of musk gland development in Chinese forest musk deer (Moschus berezovskii). Integr Zool 2024;19:955-74.
29. Flasse L, Schewin C, Grapin-Botton A. Pancreas morphogenesis: Branching in and then out. Curr Top Dev Biol 2021;143:75-110.
30. Huang L, Desai R, Conrad DN, Leite NC, Akshinthala D, Lim CM, et al. Commitment and oncogene-induced plasticity of human stem cell-derived pancreatic acinar and ductal organoids. Cell Stem Cell 2021;28:1090-104.
31. Porcheri C, Mitsiadis TA. Physiology, Pathology and Regeneration of Salivary Glands. Cells 2019;8:976.
32. Wang JH, Laurie GW. Organogenesis of the exocrine gland. Dev Biol 2004;273:1-22.
33. Barrows CML, Wu D, Farach-Carson MC, Young S. Building a functional salivary gland for cell-based therapy: more than secretory epithelial acini. Tissue Eng Part A 2020;26:1332-48.
34. Storz P. Acinar cell plasticity and development of pancreatic ductal adenocarcinoma. Nat Rev Gastroenterol Hepatol 2017;14:296-304.
35. Zhang FW, Liu Q, Wang ZY, Xie WQ, Sheng X, Zhang HL, et al. Seasonal expression of oxytocin and oxytocin receptor in the scented gland of male muskrat (Ondatra zibethicus). Sci Rep 2017;7:16627.
36. Zhang T, Peng D, Qi L, Li W, Fan M, Shen J, et al. Musk gland seasonal development and musk secretion are regulated by the testis in muskrat (Ondatra zibethicus). Biol Res 2017;50:10.
37. Li Y, Zhang T, Zhou J, Yang S, Fan M, Sun X, et al. Transcriptome analysis of muskrat scented glands degeneration mechanism. PLoS One 2017;12:e0176935.
38. Machida Y, Michishita M, Yoshimura H, Kato T, Hayama SI, Takahashi K. Malignant rhabdoid tumor of the musk gland and systemic T-cell lymphoma in a masked palm civet (Paguma larvata). J Vet Med Sci 2019;81:975-9.
39. Xu Z, Li F, Liu Q, Ma T, Feng X, Zhao G, et al. Chemical composition and microbiota changes across musk secretion stages of forest musk deer. Front Microbiol 2024;15:1322316.

Received: 31 March 2025. Accepted: 9 June 2025.

European Journal of Histochemistry 2025; 69:4216
doi:10.4081/ejh.2025.4216